THE DESIGN AND ANALYSIS OF A CONFORMAL SPIRAL ANTENNA STRUCTURE FOR AN ULTRA-WIDE-BAND RADAR SYSTEM

A Thesis
Submitted to the Graduate Faculty
of the
North Dakota State University
of Agriculture and Applied Science

By

David Benjamin Schuette

In Partial Fulfillment of the Requirements
for the Degree of
MASTER OF SCIENCE

Major Department:
Electrical and Computer Engineering

April 2016

Fargo, North Dakota

NORTH DAKOTA STATE UNIVERSITY

Graduate School

Title

THE DESIGN AND ANALYSIS OF A CONFORMAL SPIRAL ANTENNA STRUCTURE FOR AN ULTRA-WIDE-BAND RADAR SYSTEM

By

David Benjamin Schuette

The supervisory committee certifies that this thesis complies with North Dakota State University's regulations and meets the accepted standards for the degree of

MASTER OF SCIENCE

SUPERVISORY COMMITTEE:

Dr. Benjamin D. Braaten
Chair

Dr. David Rogers

Dr. Debasis Dawn

Dr. Josef Dorfmeister

Approved:

25 April 2016
Date

Scott C. Smith
Department Chair

ABSTRACT

This thesis explores the design, simulation, and analysis of two conformal spiral antenna structures that are used for an ultra-wide-band (UWB) bistatic radar. The radar antenna system operates over a frequency range from 0.9 GHz to 6.5 GHz. The UWB spiral antenna was initially derived for a planar substrate, then conformed to the spherical embodiment. A microstrip tapered balun feed structure was designed to provide a balanced signal from the radar to the antennas. This work focuses on how well the newly designed antenna system compares to the radar kit's provided planar bow-tie antennas. In particular, the comparisons between simulations and prototype measurements are presented. It is shown that a spiral antenna and structure can be conformed to a 127.0 mm diameter sphere and have little effect on the radar's performance when compared to a larger planar bow-tie antenna design.

ACKNOWLEDGEMENTS

First, I would like to thank my advisor, Dr. Benjamin D. Braaten, for his never ending support and guidance throughout this research. His encouraging and enthusiastic approach to this project was a great motivation. Without this attitude, I never would have completed this research.

Next, I would also like to thank my committee members Dr. David Rogers, Dr. Debasis Dawn, and Dr. Josef Dorfmeister for their patience and support. Their teaching styles have taught me so much about the proper approach to problem solving, overcoming difficulties, and other skills to help me become a better researcher.

Finally, I would like to thank Cyclops Technologies and everyone who made it possible for me to be able to partake in the *UAS Sensor Payload Development for Rescue Operations* research grant.

TABLE OF CONTENTS

LIST OF TABLES

LIST OF FIGURES

LIST OF SYMBOLS

ΔT ..... Time delay between a radar's transmitted signal and received reflection

δT ..... Time delay of a strobed sampler radar

d .....Distance between transmitter and receiver antennas om

v_p .....Speed of an electromagnetic wave propagating through a medium

λ .....Wavelength of a given frequency

c ..... Speed of light ($2.998(10^8)$ m/s)

L .....Distance between a radar and target object

r_i .....Inner radius of a spiral

r_o ..... Outer radius of a spiral

α ..... The flare rate of a spiral

ε ..... The expansion coefficient a spiral

ϕ ..... Number of rotations of a spiral in radians

λ_{high} ..... Wavelength of the highest operating frequency

λ_{low} ..... Wavelength of the Lowest operating frequency

δ ..... Spiral line offset

ϵ_r ..... Dielectric constant

1. INTRODUCTION

1.1. Ultra-Wide-Band (UWB) Radar Background

Radar systems have evolved immensely since their first introduction over a century ago. Newer radar systems are being developed with increasing sensitivity while decreasing in size. This has led to the development of single integrated circuit (IC) solutions for radar senors [1]. The overall size of a radar system is now being limited by the size of the antennas and not their hardware. As the miniaturization and cost of radar sensors continues to decrease, their use in commercial applications rises. This has led radar systems to be developed for unique applications such as remote heart rate monitoring, respiration rate detection, and real time through wall imaging systems [2] - [4].

One feature of ultra-wide-band (UWB) radars is its ability to detect and track a human presence from a far distance [5]. This ability is currently being developed for applications in the military, medical, and search & rescue. These systems are usually cumbersome as they require a large planar antenna system. This has inspired many research groups to create a small unique UWB antenna design that is used for specific radar applications.

1.2. Unmanned Aerial Vehicle (UAV) Project Background

This thesis work is a small part of a larger funded research project of developing a human presence detection system. The project is in collaboration Cyclops Technologies Inc.; a company specializing in providing unmanned aerial solutions for government and commercial enterprises [6]. The objective of the research project is to design and prototype a human presence detection system that will help search and rescue personnel detect victims buried in rubble. There are two primary detection systems being developed that will work in unison in the final product; (1) cell phone and (2) human presence. The cell phone detection system is an existing commercial product that is being integrated for use on an unmanned aerial vehicle (UAV). This project focuses on the through wall imaging system (TWS) that can detect and locate a buried victim. Both these detection systems will be in their own enclosures and deployed by an UAV (e.g. quadcopter). The UAV will fly over the rubble and drop multiple TWS in a grid pattern to maximize the coverage. These systems will then be able to triangulate the potential victims and wirelessly report the individual's position back to the emergency responders. By knowing the locations, the emergency personnel can

more quickly and efficiently save the victims. This system has the strong potential to be faster and more reliable than the current methods of using humans or canines to manually search a disaster site.

1.3. Novelda Background

A research and development company, Novelda, has successfully developed multiple IC sensors for UWB bistatic radar [1]. Currently, Novelda commercially manufactures and sells two of these chips; the X1 and X2. The main difference between these two products is their frequency of operation. The X1 operates between a frequency of 0.9 GHz and 6.5 GHz while the X2 operates between 4.5 GHz and 9.5 GHz. Novelda was chosen to be used for this project for its compact size and reliable performance. More specifically the Novelda X1 is used since it is theorized the lower frequencies will help the radar penetrate further into rubble. Several companies are presently using these chips in commercially available products such as ground penetrating radar (GPR) and snow depth sensors. Both the X1 and X2 work based on the concept of strobed sampling using back-scattered radiation as defined in section 1.3.3.

1.3.1. Traditional Radar Operation Theory

A brief explanation of traditional radar theory will be given as a background for the strobed sampling concept. In the simplest of configurations, a radar will have one transmitting and one receiving antenna. The transmitter will emit an electromagnetic (EM) wave that will reflect off an object of interest and return to the receiving antenna as shown in Figure 1.1.

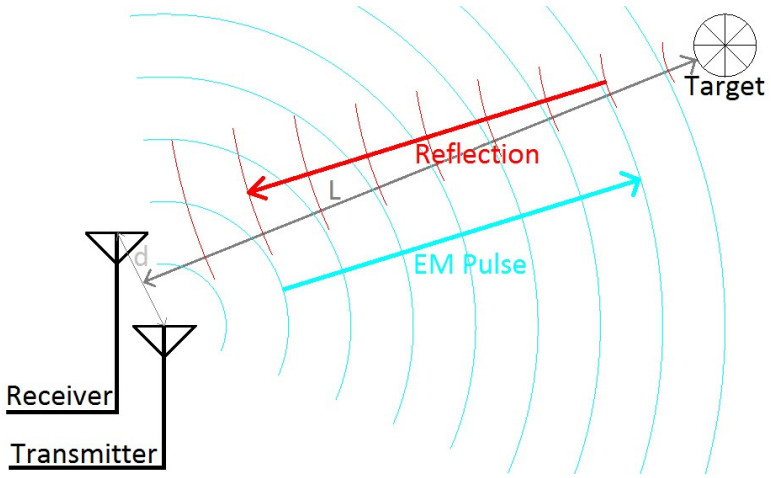

Figure 1.1. Basic radar theory diagram

In this diagram, L is the distance between the antennas and target object. d is the distance between the transmitting and receiving antenna. In many cases this distance, d, is much smaller than L. In these cases, d can be neglected in the target distance calculations. The receiver records the duration of the EM wave's time of flight. The time between the initial pulsed transmission and received reflection is defined as ΔT. The propagation velocity, v_p, of the EM wave can be used to calculate the distance, L, as shown in 1.1. In dry air, v_p is nearly equal to the speed of light, c [9].

$$L = \frac{\Delta T v_p}{2}. \tag{1.1}$$

1.3.2. Radar Definition of Terms

The Novelda X1 and X2 can both be defined as ultra-wide band (UWB) radar using a bistatic configuration. The clarification of these terms will greatly help in the explanation of strobed sampling. The definition for UWB is commonly accepted to be a bandwidth greater than 500 MHz. The X1 has a bandwidth of 5.6 GHz and the X2 has a bandwidth of 5.0 GHz.

There are two different types of radar configurations: bistatic and monostatic. These terms do not have well accepted definitions and will vary depending on the source of the work. Typically, monostatic will only have one antenna that is both a transmitter (Tx) and receiver (Rx). Bistatic will always has two antennas: Tx and Rx. The traditional radar described in section 1.3.1 is bistatic. Some sources claim that if the distance between the Tx and Rx antennas is so small that it is not accounted for in the target distance calculation; then it is considered a monostatic. The radar kit used in this project has two antennas, a Tx and Rx. However, they are only 10.0 cm apart. This 10.0 cm is not included in the data analysis algorithm. Novelda, who created both the software and hardware, defined a new term and calls it a pseudo-monostatic configuration. Since the project's focus is from a hardware/antenna design aspect, the traditional terminology will be used. For the rest of this document, the Novelda chips will be defined as a bistatic configuration simply because it requires two antennas for operation.

1.3.3. Strobed Sampling

The traditional radar described in section 1.3.1 will transmit an EM wave at a single frequency and then measure the ΔT once the signal is received. A strobed sampler will transmit a frequency band of EM waves then measure the back-scatter EM energy after a given time offset

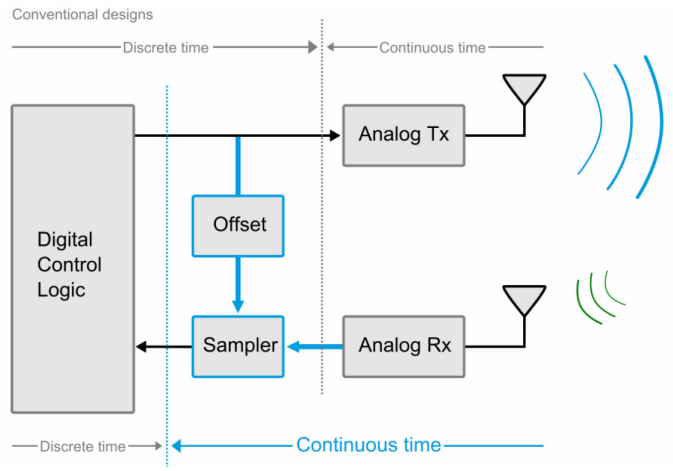

Figure 1.2. Impulse radar using strobed sampling from [7]

(δT). Unlike the traditional radar, this time offset is predefined. Figure 1.2 shows a block diagram of this concept [7].

By measuring the background radiation, the radar will detect which frequency bands are reflected off the target object. Using the propagation velocity, v_p, and the offset time, δT, the distance to the target object, L, can be calculated using [7]:

$$L = \delta T v_p. \tag{1.2}$$

The unique property of strobed sampling is that it can scan progressively over a distance, whereas traditional radar will only measure a reflection when a target object is acquired.

The Novelda X1 chipset, used in this project, uses 512 parallel samplers. After the transmitted signal is emitted; the chip will wait an offset duration, δT. As shown in (1.2), δT is directly related to L. The longer the offset time, the further distance the EM waves will have traveled. The propagation velocity of the EM wave is crucial to accuracy of the calculated distance. The reference distance, RD, is the distance at which the radar will start scanning and is equal to L. After the offset time, the chip will then take in 512 samples in rapid succession. Since each sample will have an offset time of its own, each time the chip takes in a sample, it is actually measured over a certain distance defined as SD (Sample Distance). Figure 1.3 shows a bistatic radar using strobed sampling to measure the distance to an object [7].

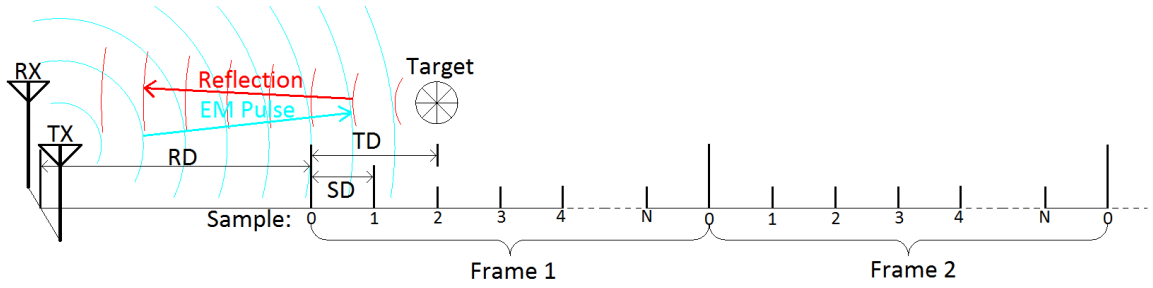

Figure 1.3. Distance from radar to target object using strobed sampling

The total distance to the target object is the sum of *RD* and *TD* (Target Distance after reference). *N* is the number of samples minus one. *SD* is related to the number of samples taken in one second. To measure over greater distances, a feature called framestitch can be used. Figure 1.3 shows a framestitch value of two. After sampling/sweeping frame 1, *RD* will automatically adjust its time delay, δT, to line up the first sample of frame 2 with the last sample of frame 1. This process can be repeated up to 15 times on the X1. The more frames added, the longer the device will take to complete a sweep, but the farther distance the radar will scan. There are several variables of the X1 that can be adapted to find the balance between speed and accuracy for a specific hardware/antenna design. This software optimization is part of a future phase of the UAS research project and is not discussed in this thesis.

1.4. Flat Earth Inc. Development Kits

Novelda recognizes their chips have strong potential use in a wide variety of life saving products, and they are committed to creating an open-source community encouraging entrepreneurs, research institutions, and commercial companies to come up with innovative uses of their radar chips. Novelda only make and support the X1, X2, and the Inspiration Kit. A radar hardware development company, Flat Earth Inc., has teamed up with Novelda and manufactures development kits for both the X1 and X2. These kits feature open source software, called Salsa, and SMA connected antennas [8]. The Cayenne radar development kit, pictured in Figure 1.4, was chosen because it was a commercially available development kit that featured the X1 and had detachable antennas. Flat Earth's radar hardware runs on a Beagle Bone Black (BBB) and are compact in size. The BBB allows for real-time data analysis as well as easier transmission of the data back to a central user. The provided bow-tie antenna system, along with Salsa software, is capable of through wall human presence detection without any aftermarket configuration.

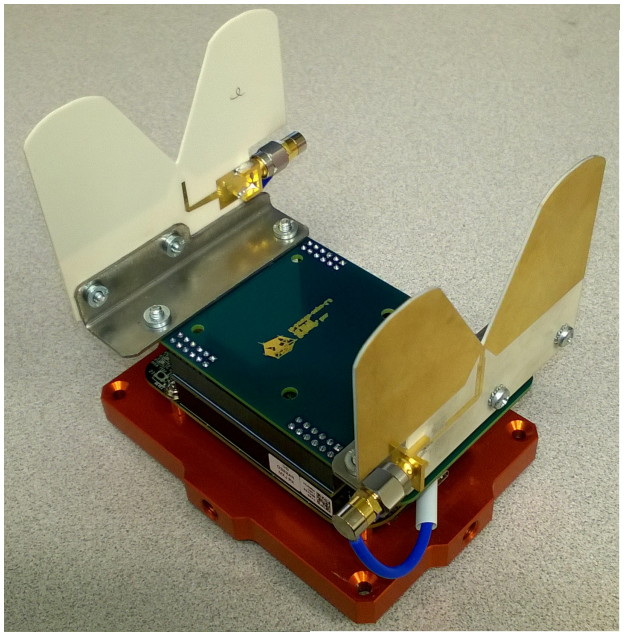

Figure 1.4. Fully assembled Cayenne radar development kit.

1.5. Purpose of Thesis Work

The Cayenne kit's antennas, described in section 1.4, do not meet the size requirements for the unmanned-aerial-system (UAS). A new UWB antenna needed to be designed to conform to the proposed embodiment of the detection system. The Cayenne radar will need to be housed in a small sturdy enclosure that can withstand the forces of the drop to the ground from a UAS platform. The radar along with the Beagle Bone Black (BBB), pictured in Figure 1.5, and a battery powered pack will need to be included in the embodiment. The first prototype was chosen to be a 127.0 mm diameter sphere. This initial size allows us to easily fit an unmodified BBB, Cayenne radar, and battery pack in a single embodiment to provide a proof of concept.

More specifically, this work explores the design of a spiral antenna and feed structure. This design was mathematically derived, simulated, and validated through $|S_{11}|$ and gain measurements of a manufactured prototype. The $|S_{11}|$ is the power reflected at the input port of an antenna. This measurement is used to define the antenna's bandwidth. The gain of an antenna is the ratio of power being transmitted in the far-field compared to the input power. The antenna was then integrated with the Cayenne radar system. This spiral design differs from others in that it is conformed to a spherical structure. Along with the validation of the antenna itself, the integration and use of the antenna will also be explored. Two antennas are needed on the surface of the embodiment as the

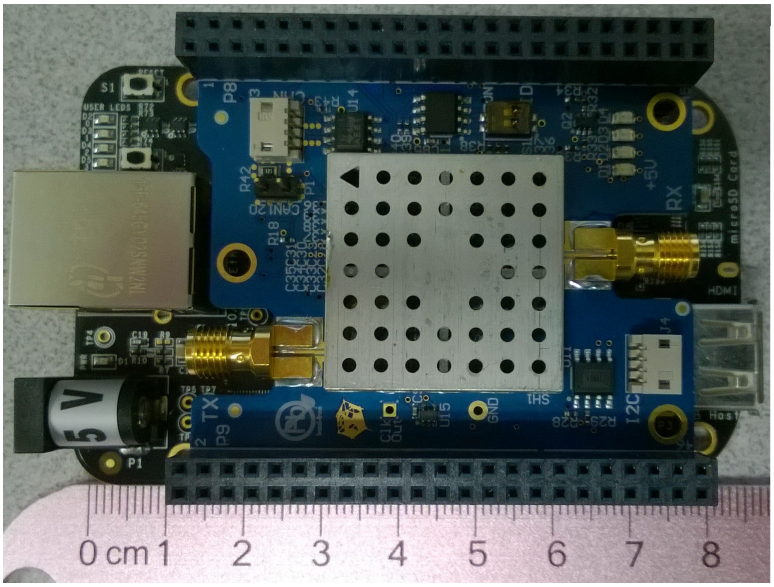

Figure 1.5. Beagle Bone Black (BBB) with Cayenne radar attached (no antennas)

radar system is a bistatic configuration. The two identical spiral antennas were initially designed on a planar substrate. This dual antenna design was then conformed to a spherical structure that has a radius less than a wavelength of the radar's center frequency. For the first time, an antenna system for an UWB radar is integrated into a spherical embodiment.

2. DERIVATIONS AND SIMULATIONS OF SPIRAL ANTENNA

2.1. Introduction

This chapter looks at the mathematical derivation and HFSS simulation of the spiral antennas. The design of a two-arm equiangular spiral antenna is derived and simulated over the frequency range of 1.0 GHz to 10.0 GHz. It is shown that a spiral antenna with outside diameter of 47.76 mm can have a simulated -10 dB bandwidth of over 8.0 GHz. The antenna was first designed and simulated as a planar structure. This structure was then adapted to a convex shape on a hemispherical surface that has a diameter of 127.0 mm.

2.2. Spiral Antenna Background

The Cayenne radar module operates at a frequency range of 0.9 GHz to 6.5 GHz and requires the use of two UWB antennas. The Cayenne development kit was provided from the manufacturer with two planar bow-tie antennas. The goal was to match or improve the performance of the planar design using an antenna built into the spherical embodiment of the through-wall-imaging system (TWS). After research and preliminary testing, it was decided a spiral would be a good candidate to achieve this goal. Common UWB antenna designs, such as the Vivaldi or bow-tie, strongly rely on its planar structure to operate over a wide band. It was shown in simulations that a minimal conformation around a large diameter cylinder would cause these antennas to have very high return loss when compared to their planar counterparts. Another problem with these antenna designs is they radiate toward the end of the printed circuit board (PCB). The sinuous and spiral antennas both radiate perpendicular to the PCB as desired if attached to the outside of a sphere. A two-arm equiangular spiral antenna design was primarily chosen for this application for its easily defined shape and UWB characteristics. Conical and planar spirals have been widely used for well over a decade. Very little research has been conducted on conforming a spiral shape over a convex sphere. By comparing the planar to the conformed results, the effects of conforming can be explored.

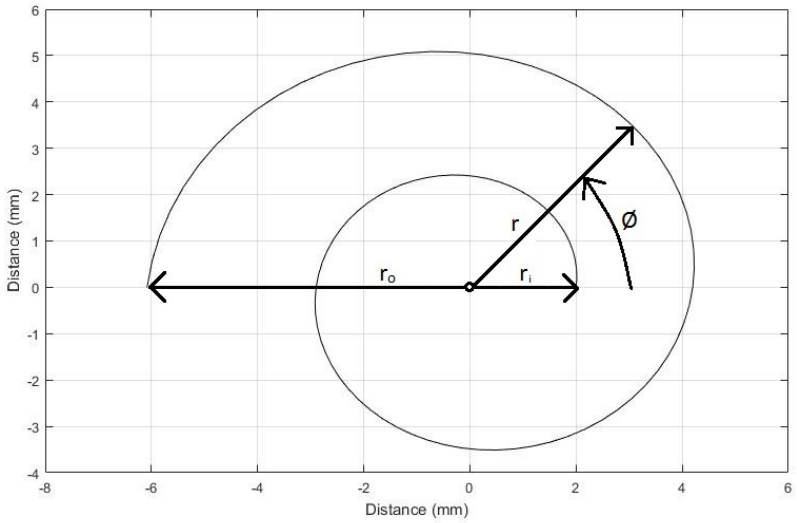

Figure 2.1. Spiral plot with $r_i = 2.0$ mm and $\alpha = 0.118$

2.3. Mathematical Derivation of Spiral Shape

The design of the spiral follows the same methods shown in [9] and [10]. The equation of the single spiral line plotted in Figure 2.1 is the following:

$$r_1 = r_i e^{\alpha(\phi)} \tag{2.1}$$

where r_1 is the distance from the center to a given point on the spiral [9]. r_i is the initial starting radius. The flare rate, α, is a constant that controls how quickly the spiral expands. The flare rate is related to the expansion coefficient, ε, as shown as:

$$\varepsilon = e^{\alpha 2\pi}. \tag{2.2}$$

ϕ is the angle of vector r in relation to the positive x direction [9]. Because of this, ϕ represents the number of rotations in radians. For example, in Figure 2.1, ϕ is plotted from 0 to 3π. Since 2π is one rotation of a circle, 3π is 1.5 rotations.

To create a tapered planar spiral surface, an offset (δ), was placed in (2.1) and is:

$$r_2 = r_i e^{\alpha(\phi-\delta)}. \tag{2.3}$$

A common design will have δ equal $\pi/2$ to create pattern symmetry. This offset was used in this work. To create a two arm spiral, the plane was copied and rotated by π radians. This offset is included in the following equations:

$$r_3 = r_i e^{\alpha(\phi-\pi)} \tag{2.4}$$

$$r_4 = r_i e^{\alpha(\phi-\pi-\delta)}. \tag{2.5}$$

Figure 2.2 shows the plotted output of all four equations for $r_i = 2.0$ mm, $\alpha = 0.118$. This particular spiral shape has the ends squared off. These edges are typically tapered to a point as needed to provide a clean termination. The center of the spiral is also tapered to a single point to prevent a large impedance mismatch between the feed structure and antenna as these spiral designs are fed from the center.

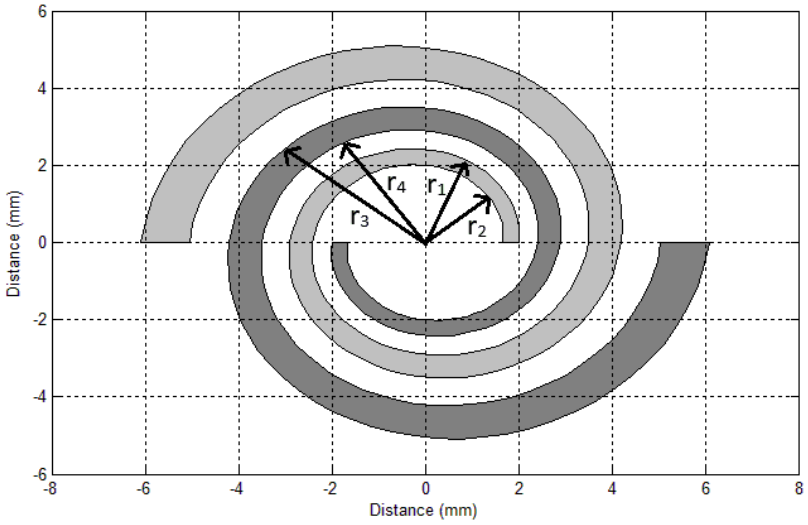

Figure 2.2. Two arm spiral plot with $r_i = 2.0$ mm, $\alpha = 0.118$, $\delta = \frac{\pi}{2}$

The inner and outer radius equations for an equiangular spiral antenna are the following equations:

$$r_i = \frac{\lambda_{high}}{4} \tag{2.6}$$

$$r_o = \frac{\lambda_{low}}{4\pi} \tag{2.7}$$

where λ_{high} is the wavelength of the highest operating frequency and λ_{low} is the wavelength of the lowest frequency [10].

The radar's operating frequency is from 0.9 GHz to 6.5 GHz. Using (2.6) and (2.7) for these frequencies yields r_i = 11.5 mm and r_o = 23.88 mm. The number of turns and expansion coefficient were found to be 3.36 and 2.1, respectively, through simulation iterations to minimize the return loss.

2.4. HFSS Comparison of Planar Spiral Simulations

The antenna shape with the parameters given in section 2.3 was simulated on a 20 mil thick Rogers RT/duroid 5880 substrate with 0.5 oz/sqft copper cladding (ϵ_r = 2.2, tanδ = .0009) [11]. This substrate was chosen for its low dielectric constant and physical flexibility. The flexibility of the material is critical as it will need to conform to the sphere. The spiral was simulated to optimize the return loss. The flare rate and radius was modified until the $|S_{11}|$ was at it's lowest in the frequency band of interest (0.9 GHz to 6.5 GHz). The final values are the same given in section 2.3.

The antenna was compared to an HFSS simulation of Flat Earth's bow-tie antenna. The validation of the bow-tie design was done through HFSS simulation and PCB measurements. Flat Earth Inc., who was very cooperative, did provide the properties of the material used. However, they would like their design to stay proprietary. Out of respect for their design and cooperation, the physical design dimensions and material used will not be mentioned. However, the results of the simulations and measurements will be shown to give a baseline for the spiral antenna validation. Figure 2.3 (b) is the top copper plane of the HFSS bow-tie model and is fed by a 50 Ω port located on the lower right side. The bow-tie includes a tapered balun structure located on the bottom plane.

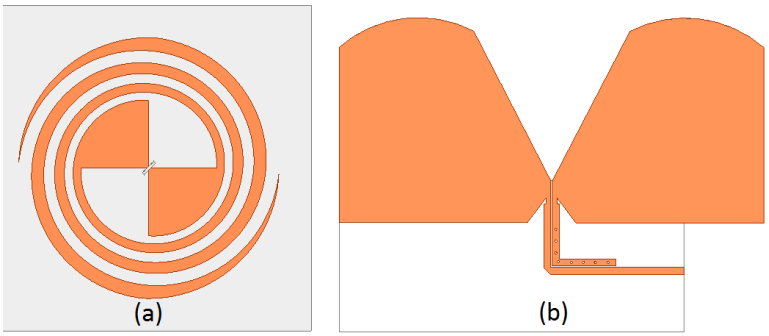

Figure 2.3. HFSS model of (a) spiral and (b) bow-tie

The spiral, with dimension given in section 2.3, is pictured in Figure 2.3 (a). In this simulation model, the spiral is fed from the center. The simulations found the port impedance to be 127 Ω. The lumped port model was updated to match this impedance and the $|S_{11}|$ and gain measurements were taken.

An interpolating sweep was used in HFSS from 1.0 GHz to 10.0 GHz using a lumped port model. As shown in Figure 2.4, the spiral had a -10 dB bandwidth of over 8.0 GHz while the bow-tie had a maximum bandwidth of 3.5 GHz.

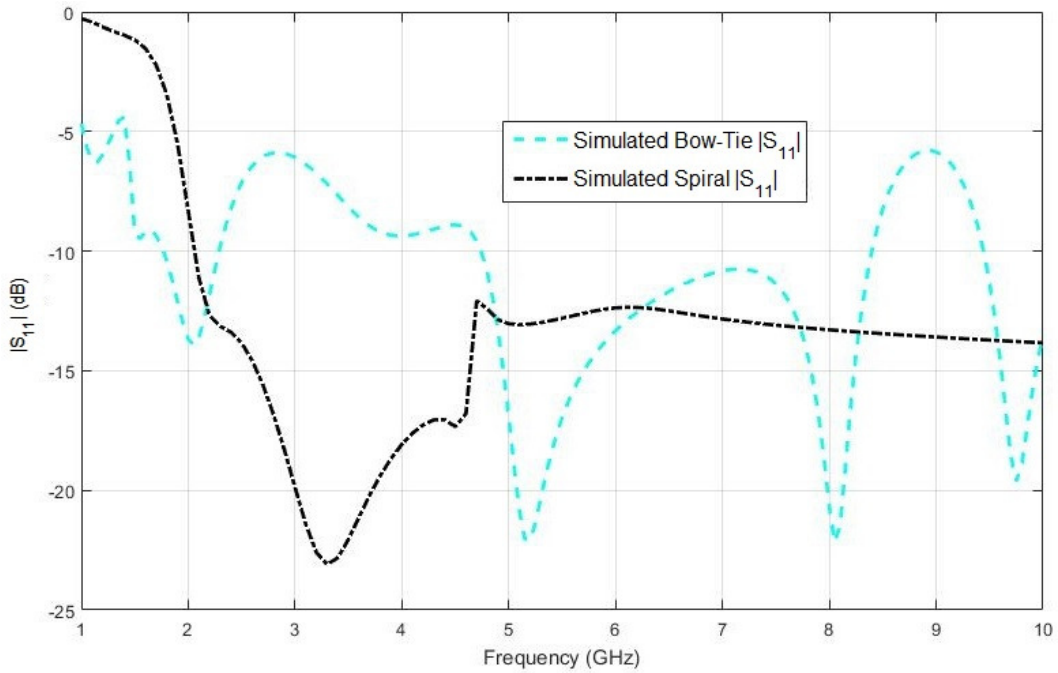

Figure 2.4. $|S_{11}|$ comparison for HFSS simulated bow-tie and spiral antennas

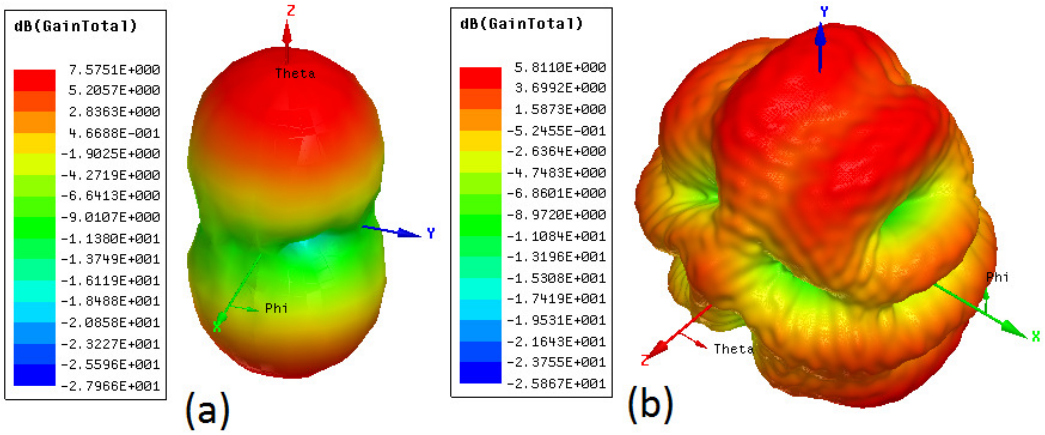

Figure 2.5. 3D gain plot of (a) spiral and (b) bow-tie antennas

The 3D polar gain plots of the spiral and bow-tie are shown in Figure 2.5 (a) and (b), respectively. Both antennas were modeled on the x-y plane. The spiral antenna had a peak gain of 7.58 dB in the both the positive and negative z directions. The bow-tie had a peak gain of 5.81 dB in the positive y direction. When comparing the two simulation results, the spiral had higher gain, lower return loss, and larger bandwidth, all of which are desirable characteristics for an UWB radar antenna.

Figure 2.6 (a) is the polar gain plot of the spiral antenna with a θ cut at $\phi = 90$ degrees. The gain plot was taken during a simulation where both antennas were powered simultaneously. Figure 2.6 (b) is the gain plot of the bow-tie with a ϕ cut at $\theta = 90$ degrees. These plots show the spiral is more directional than the bow-tie.

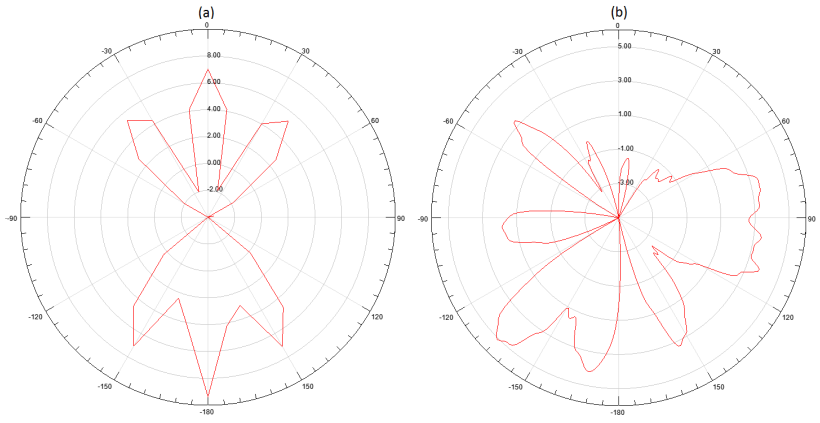

Figure 2.6. 2D polar gain plot of (a) spiral and (b) bow-tie antennas powered

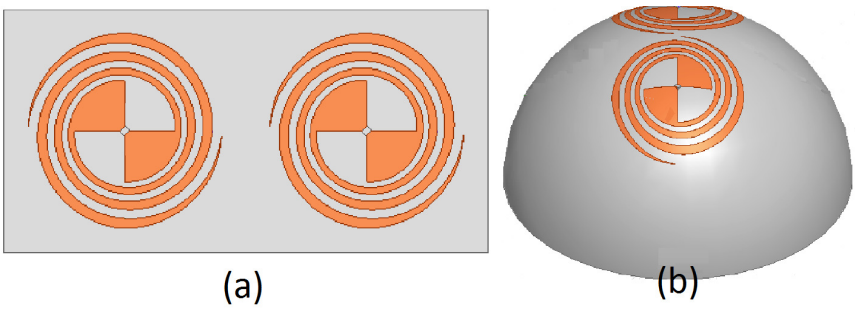

Figure 2.7. (a) Planar two arm spiral antenna (b) Same dimensions conformed to hemisphere

2.5. HFSS Comparison of Convex Spiral Simulations

The spiral design from the previous section was duplicated with a spacing of 5.0 mm. This shape was then superimposed onto a 127.0 mm diameter sphere. The sphere has the same Rogers RT/Duroid 5880 substrate as used in the previous simulations and the inside of the sphere was hollow (air). Figure 2.7 shows a side by side comparison between the planar spiral and convex hemispherical.

The simulated $|S_{11}|$ of the conformal antenna compared to the planar and bow-tie is shown in Figure 2.8. According to the HFSS simulation, the spiral will have a much lower $|S_{11}|$ when conformed than when planar.

Figure 2.9 (a) shows the 3D gain polar plot comparing the the conformal system when simulated when both antennas are radiating and one antenna radiating is shown in Figure 2.9 (b). The gain plots show a peak gain of 8.54 dB in the z direction for the dual-transmitting structure. The single transmitting spiral had similar gain but the peak radiation was off-centered.

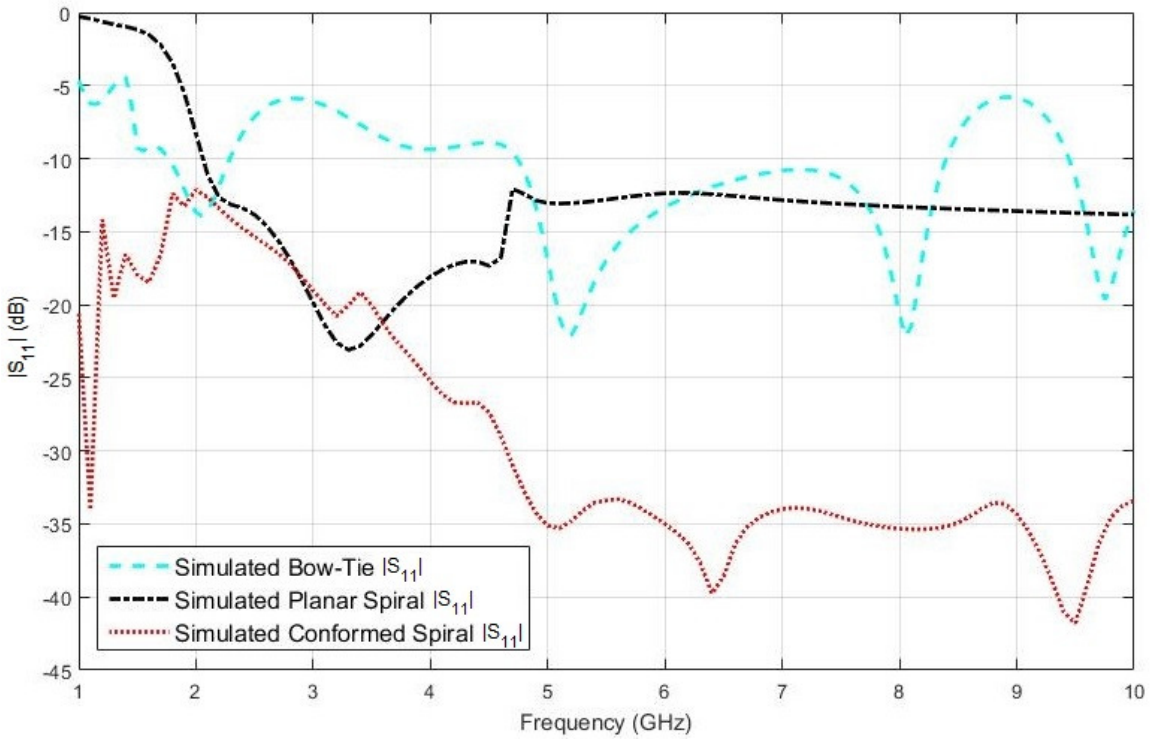

Figure 2.8. $|S_{11}|$ comparison between conformed spiral, planar spiral, and bow-tie antennas

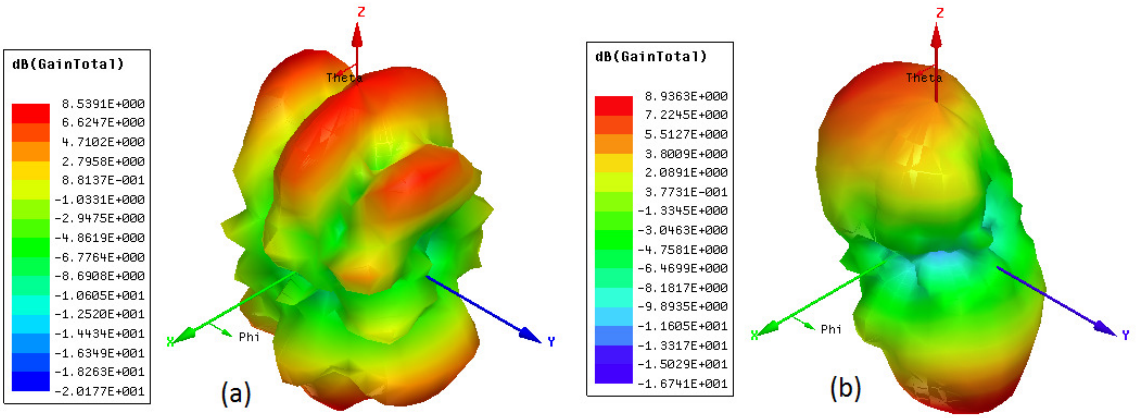

Figure 2.9. 3D polar gain plot of convex spiral antennas with (a) both simultaneously transmitting (b) one transmitting

3. DERIVATION AND SIMULATIONS OF BALUN TRANSFORMER

3.1. Introduction

This chapter explores the design and simulation of the feed structure for the spiral antenna. A microstrip tapered balun impedance transformer was designed and simulated in HFSS. It is shown the taper balun is capable of a impedance transformation from 50 Ω to a 127 Ω with a 180 degree phase difference and a loss ,$|S_{12}|$, less than -3 dB over the frequency band from 1 GHz to 10 GHz.

3.2. Background of Tapered Balun

Due to the nature of the design, a dual-arm spiral antenna requires a balanced input. There are single integrated circuit (IC) chip baluns available; none of these would meet the 0.9 GHz to 6.5 GHz bandwidth requirements. Wire wound ferrite core UWB impedance transformer baluns are also common. These are typically large in size and are unforgiving in design due to the number of errors that can take place during manufacturing. The microstrip balun design is another popular design that is integrated with an impedance transformer. The total length can be designed to be less than a quarter wavelength of the center frequency. The low loss and UWB characteristics are the primary reasons for which this design was chosen.

3.3. Tapered Balun Design Dimensions

The goal was to connect the antennas to a 50 Ω unbalanced coaxial cable that will be attached to the radar. To accomplish this task, a back-to-back tapered microstrip-to-parallel strip balun design was used. It can be shown that an ideal self complementary spiral antenna has an input impedance of 188.5 Ω [10]. Through simulation, the input impedance of the antenna was found to be approximately 127 Ω. The balun transformer dimensions were derived using the same methods as shown in [13] and equations from [15]. Two designs were simulated and tested on 62 mil thick Rogers RT/Duroid 5880 substrate [11]. The top and bottom copper plane designs of the structure are shown in Figure 3.1 (a) and (b), respectively.

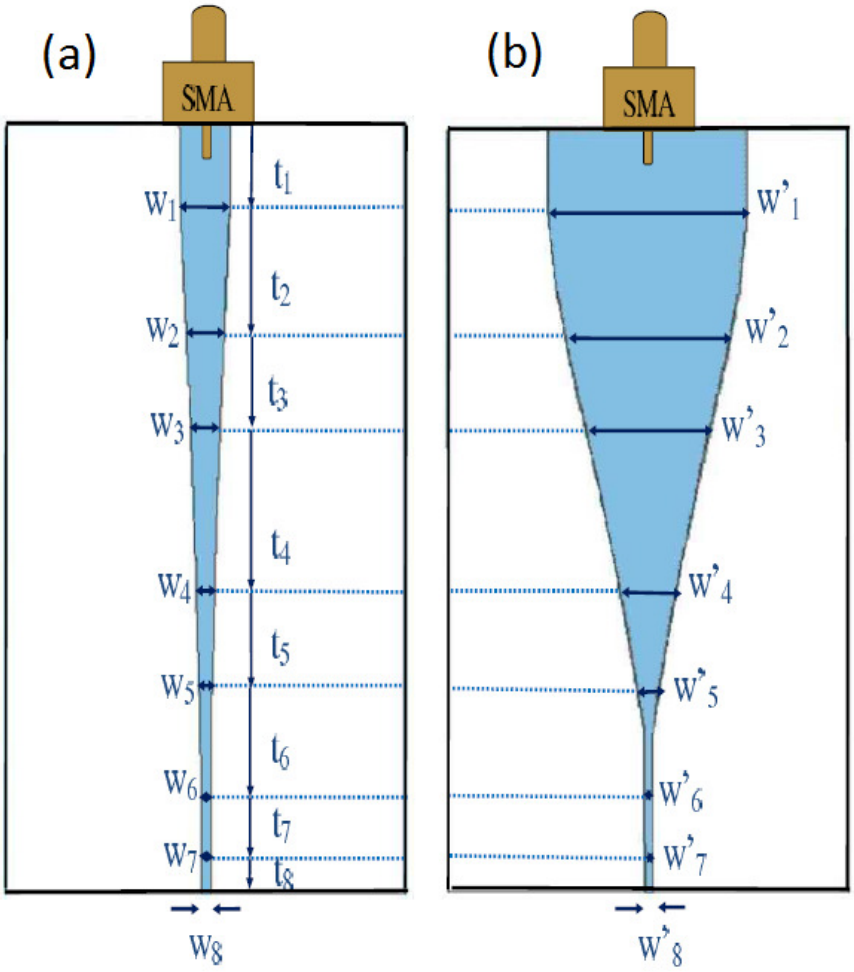

Figure 3.1. Dimension for top (a) and bottom (b) copper plane for the balun structure [13]

Table 3.1 gives a side-by-side comparison of the structures (1) and (2) dimensions in reference to Figure 3.1. Structure (1) uses the same dimensions as provided in [13]. This was done to validate their research as well as providing a baseline for the modified design; structure (2). The difference between the two is the impedance transformer. Structure (1) was designed for a 50 Ω to 180 Ω transformation. Structure (2) was designed for 50 Ω to 120 Ω transformer. Structure two dimensions were derived using the same methods shown in [13].

3.4. Tapered Balun Design Simulation Results

The simulations of the balun design did not exactly match the results from [13]. Their simulations used Computer Simulation Technology (CST) [14]. Then it was validated by connecting it to a known antenna design. Their method of simulation was taking two of the balun structures and connecting them together as shown in Figure 3.2 (a).

Table 3.1. Comparison between structure (1) and (2) balun dimensions.

i	Structure (1) W_i (mm)	Structure (1) W_i' (mm)	Structure (2) W_i (mm)	Structure (2) W_i' (mm)	Structure (1) t_i	Structure (2) t_i
1	4.80	18.0	6.10	22.9	5.00	5.00
2	2.60	16.0	3.30	20.3	12.7	17.8
3	1.76	7.00	2.24	8.90	22.2	33.7
4	1.20	2.00	1.53	2.54	29.8	46.3
5	1.10	1.80	1.40	2.29	41.5	65.8
6	0.92	0.98	1.17	1.25	46.2	73.7
7	0.88	0.88	1.12	1.12	50.0	80.0
8	0.88	0.88	1.12	1.12	70.0	85.0

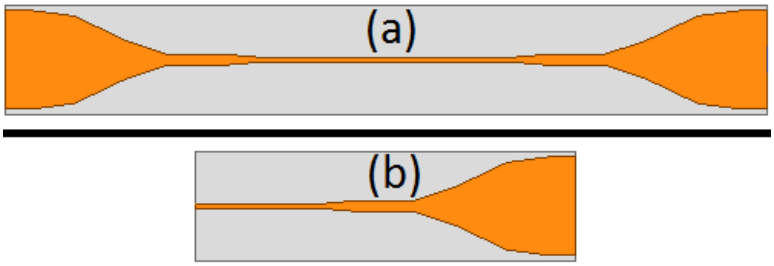

Figure 3.2. (a) Two tapered baluns placed back-to-back (b) Single tapered balun

The two ports had 50 Ω impedance. A current probe was placed over the top and bottom copper planes in the middle of the PCB perpendicular to the trace. It was shown the current on the top plane was 180 degrees out of phase to each other. To simulate the impedance loss through the transformer, a single balun was placed with one port impedance set to 50 Ω and the other to 127 Ω, as shown in Figure 3.2 (b). $|S_{12}|$ had a maximum of -1.19 dB of loss as shown in Figure 3.3.

This balun is not ideal and does introduce loss into the system. However, it should be noted the design could be a little off; thus, the 127 Ω port might not be a perfect match, resulting in larger loss. This could be perfected in simulations, but the actual prototype PCB antenna might not be a perfect 127 Ω either. Therefore, these two structures, (1) and (2), were milled and validated through PCB measurements.

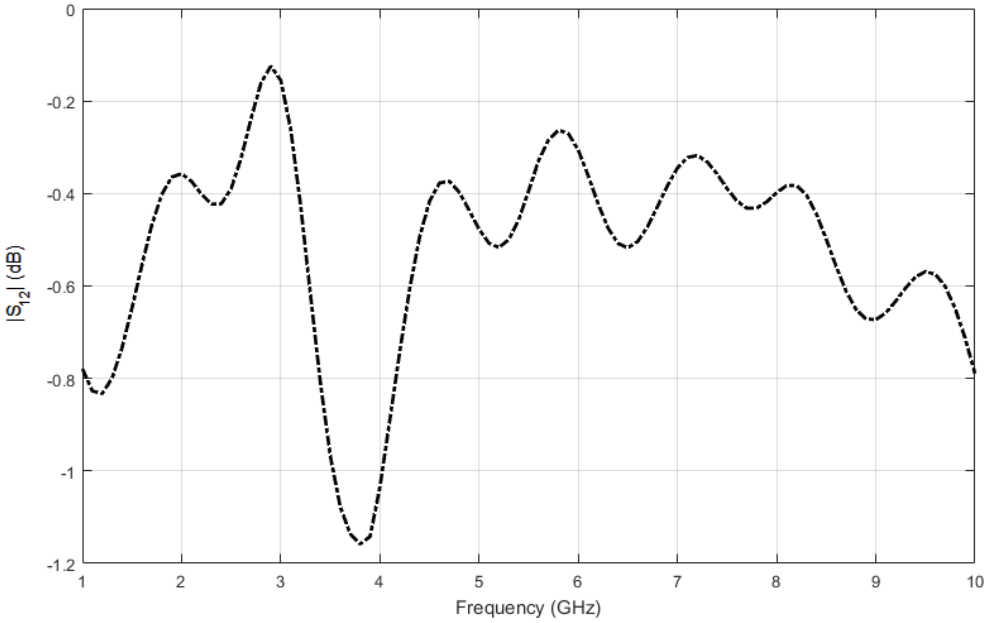

Figure 3.3. $|S_{12}|$ of the tapered balun structure (2)

4. VALIDATION OF SIMULATIONS THROUGH MEASUREMENTS

4.1. Introduction

In this chapter, the results of the measured prototypes are compared to the HFSS simulations shown in Chapters 2 and 3. The gain and $|S_{11}|$ measurements are the main figures of merit for these comparisons. It is shown the measurements are similar to the simulations, but not similar enough to accurately predict the antenna's bandwidth.

4.2. Design of Hemisphere Surface

A prototype of the 127 mm diameter sphere was 3D printed. Unlike the simulations, the sphere was constructed out of plastic and only the area under the antennas had the 20 mil thick Rogers RT/Duroid 5880 [11]. The sphere's wall thickness is 5 mm and were hollow to save on printing material and time. The shell thickness of the wall was 1 mm. The material is a typical polylactide (PLA) plastic commonly used for various 3D printing applications. The antennas with the 20 mil Rogers RT/Duroid substrate were attached to the outside of the sphere using double-sided tape. The constructed prototype sphere bottom and top are pictured in Figure 4.1 (a) and (b), respectively. In this picture, the feed structures are hidden since they are perpendicular to the antennas and fed through a small hole to the inside of the sphere. This conformal sphere setup was used for all spiral measurements described in the following sections.

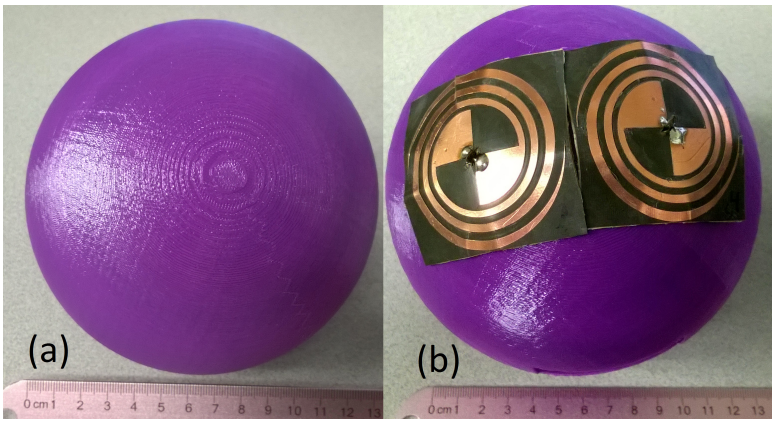

Figure 4.1. (a) Bottom of sphere (b) Top of sphere with antennas attached

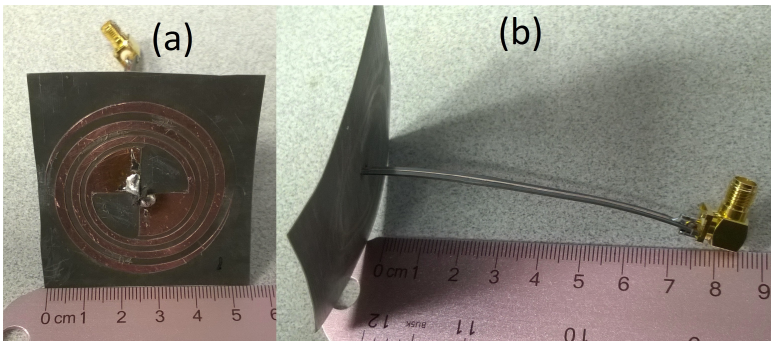

Figure 4.2. (a) Single planar spiral antenna (b) Taper balun feed structure

4.3. Feed Structure Measurements

Four identical spiral antennas were milled using the same dimension and material as the simulations. Both of the structure designs discussed in chapter 3 were also manufactured. To validate and compare the two designs, the feeds were connected to a planar antenna, and the $|S_{11}|$ values were measured. Figure 4.2 (a) is a picture of an individual planar spiral antenna with a feed structure. Figure 4.2 (b) shows how the feed structure is attached through the bottom of the antenna.

The measured results indicate structure (1) provided a lower return loss over the desired bandwidth when attached to the spiral antenna. This structure was chosen to be used for the final design. The $|S_{11}|$ comparing both feed structures for a planar and spherical spiral antenna is shown in Figure 4.3.

4.4. $|S_{11}|$ and Gain Comparison Measurements

The Cayenne radar development kit was provided with an UWB bow-tie antenna system that works well for through wall presence detection. However, they are too large for the desired spherical embodiment needed for the UAS system. All measurements are compared using the bow-tie antennas as the desired standard. Both $|S_{11}|$ and the gain measurements were taken of the antenna systems over the frequency range from 1 GHz to 10 GHz. Figure 4.4 shows the simulated conformal spiral has a lower $|S_{11}|$ than the simulated bow-tie antennas. The measured -10 dB bandwidth of the convex spiral is 3 GHz starting around 2 GHz. The measured bow-tie bandwidth was 5.9 GHz, almost twice the value of the spiral's, but it does not drop below -10 dB until 2.8 GHz. The spiral design provides a lower return loss at the lower frequencies while the bow-tie is lower at the higher frequencies. Choosing between these trade-offs is strongly dependent on the application

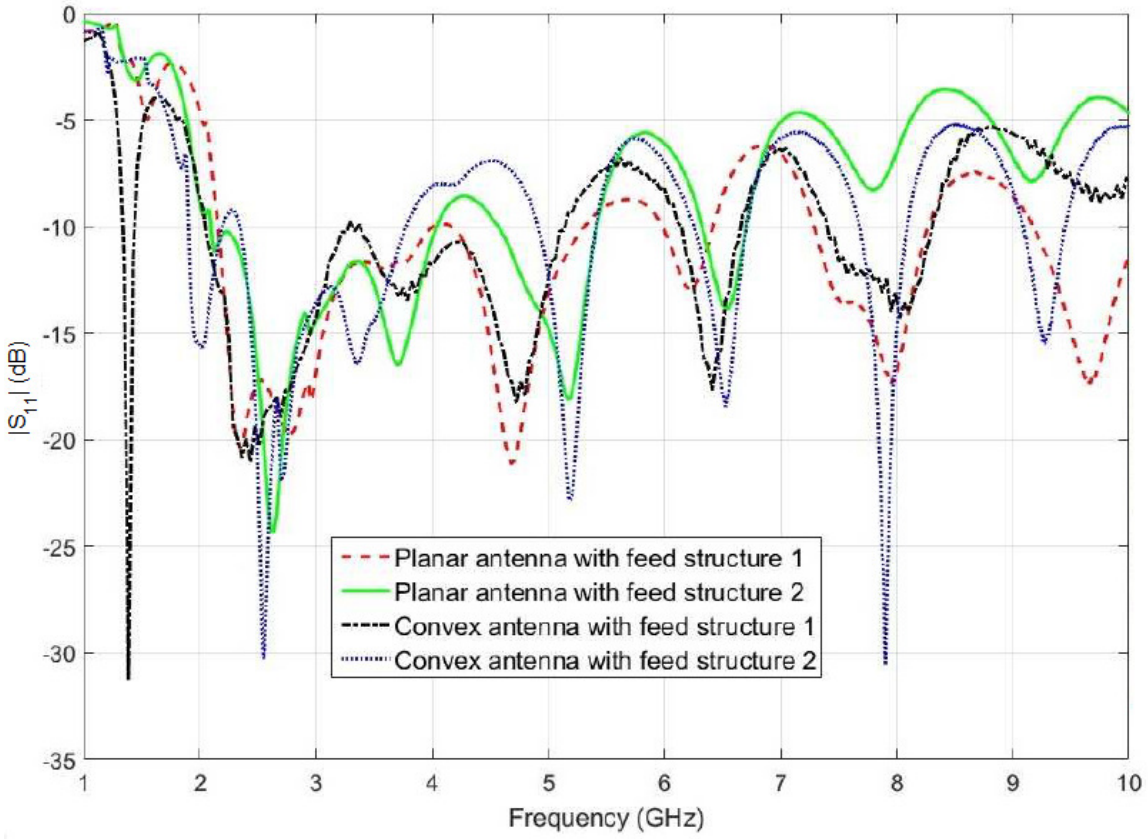

Figure 4.3. Measured $|S_{11}|$ of spiral antenna comparing feed structures (1) and (2) for both planar and convex antennas

of the Cayenne radar system. Lower frequencies are desired for better material penetration. The simulation outputs for both antennas were near the measured values. However, the simulations did not provide accurate -10 dB bandwidths.

The gain measurements were then taken in a RF anechoic chamber as well as simulated in HFSS in the 1 GHz and 10 GHz frequency range. The HFSS simulated 3D polar gain plot of the spiral and bow-tie are shown in Figure 4.5 (a) and (b), respectively. Figure 4.5 (c) and (d) demonstrate the orientation of the gain plots with respect to the model. In Figure 4.5, (a) and (c) are aligned for the spiral; (b) and (d) are aligned for the bow-tie.

The gain was measured using a TDK 1 GHz - 18 GHz horn antenna placed one meter away from the antenna under test as shown in Figure 4.6 (a). The positions of the peak gain in simulations were used when taking the PCB measurement. The bow-tie was perpendicular to the horn antenna as shown in Figure 4.6 (a). The spiral dome structure was placed with the top facing the horn antenna. Figure 4.6 (b) is a picture of a bow-tie $|S_{11}|$ measurement.

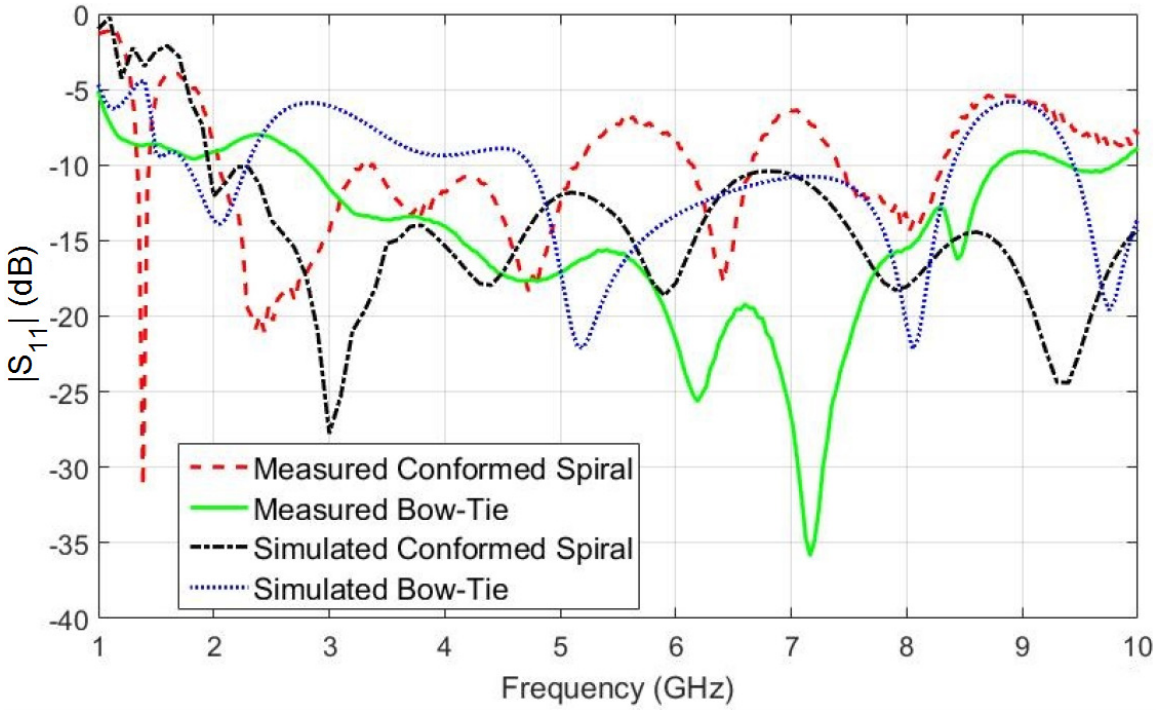

Figure 4.4. Comparison between measured and simulated $|S_{11}|$ for both spiral and bow-tie antennas

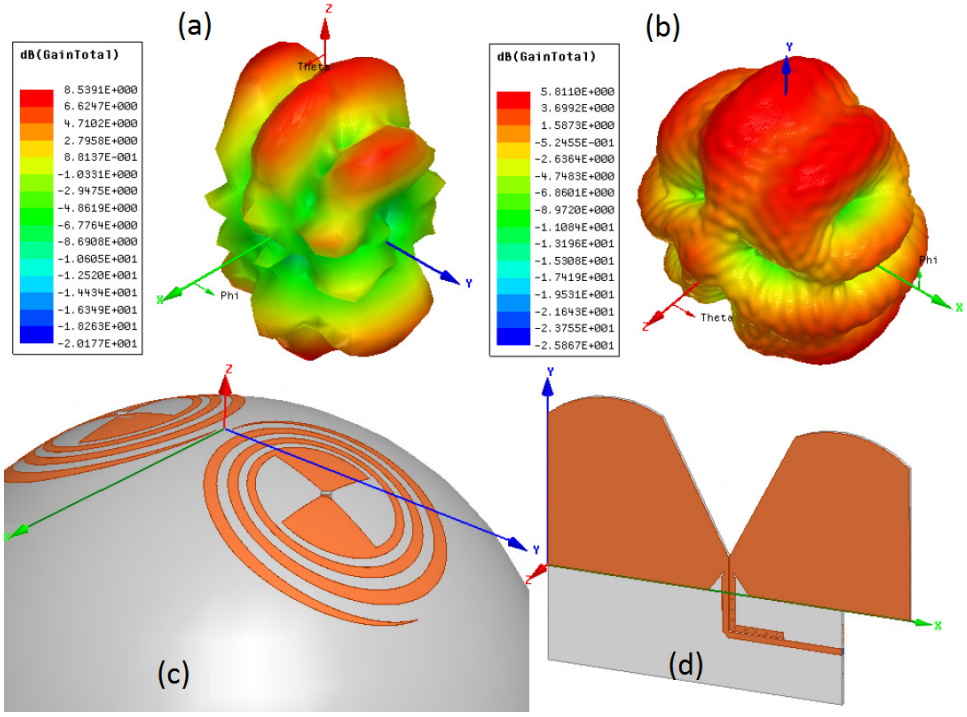

Figure 4.5. (a) Spiral simulated 3D gain plot (b) Bow-tie simulated 3D gain plot (c) Spiral HFSS model (d) Bow-tie HFSS model

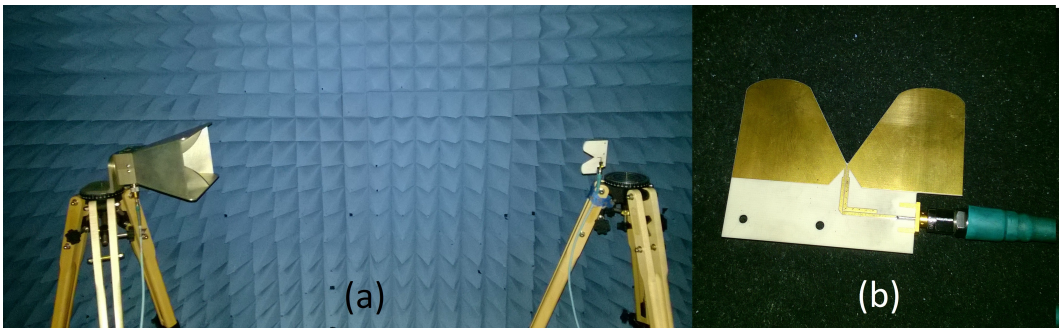

Figure 4.6. (a) Gain measurement using horn and bow-tie antenna (a) $|S_{11}|$ measurement of bow-tie antenna

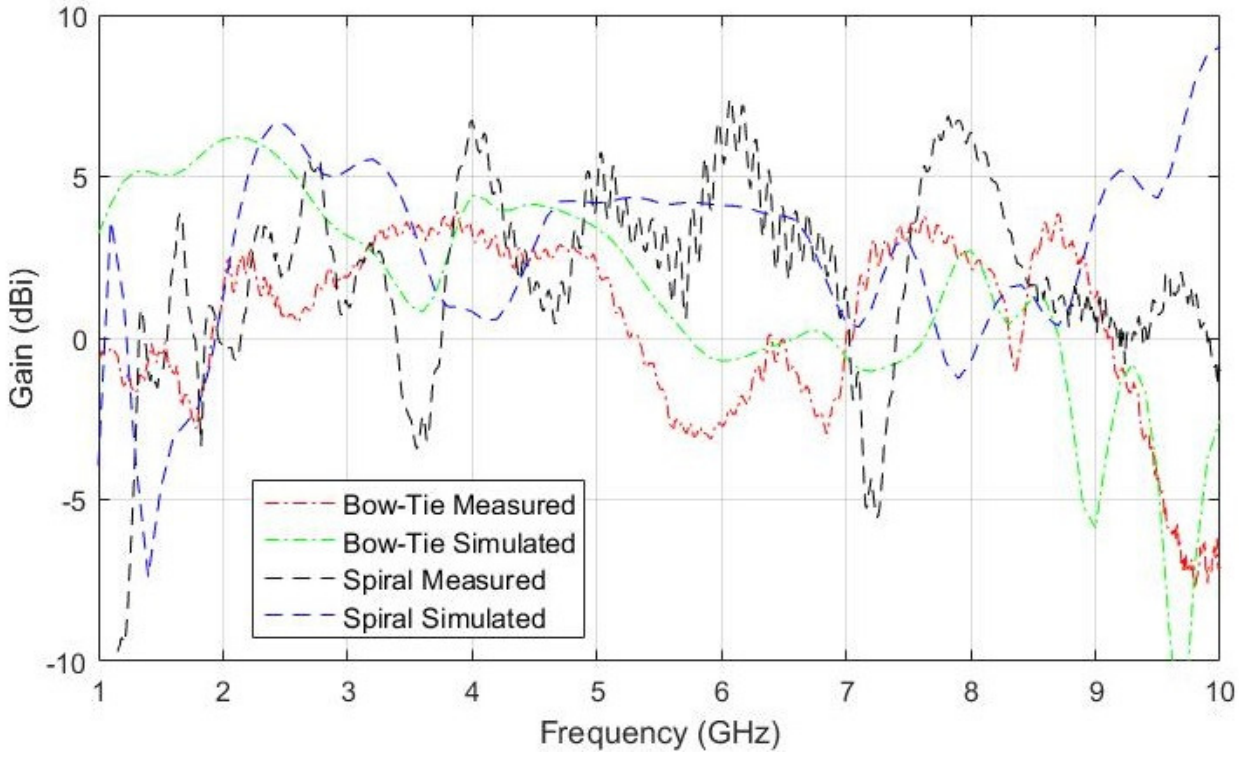

Figure 4.7. Comparison between measured and simulated gain for both spiral and bow-tie antennas

The comparisons between the peak gain between the simulated antennas and measured antennas are shown in Figure 4.7. The MATLAB code and gain equation that was used for this plot is shown in the Appendix. The simulated gain did not provide an accurate prediction of the measurements. The measured gain of the spiral is lower than the bow-tie's below 4.9 GHz. In summary, the spiral had lower $|S_{11}|$ and gain for the lower half of the radar's frequency bandwidth. The lower gain may not be ideal, but the lower $|S_{11}|$ is desired.

5. INTEGRATION OF ANTENNAS WITH RADAR SYSTEM

5.1. Introduction

So far in this project, a spiral antenna with a taper balun feed structure has been designed, simulated, and measured. These measurements were compared to the simulated and measured results of the Cayenne radar's bow-tie antennas. Since the goal of this work was to design a conformal antenna system that will be used with the Cayenne radar; the true validation of this proposed antenna structure is to compare radar measurements. Below is a summary of this comparison testing. It should be stated the purpose of this particular test is to only compare the two different antenna systems. Thus, it was not meant to test the software, penetration capabilities, nor the sensitivity of the radar itself.

5.2. Initial Through Wall Testing

Initial testing was conducted in a vacant office building. The radar was placed against a wall in one room while a person would go into the adjacent room and take a B-scan using the Salsa software. A B-scan plots the voltage value of radar samples taken in over a duration of time. This voltage value is the strength of the received signal of the radar. A B-scan plot will map the area of interest over a certain range and time period. The test subject would stand in predetermined positions around the room, and the B-scan measurements were compared. The two antenna systems showed similar B-scans and voltage reading for each position. However, this was determined to be a very unreliable way of completing these measurements, and the approach described in section 5.3 was more accurate. The reason these results were mentioned was to confirm these spiral conformal antennas can function as a through wall human detection system.

5.3. Through Wall Testing Setup

The more favorable approach to demonstrating radar systems is to sweep the radar along a wall or obstruction and see how accurately it can detect an object on the other side. The two primary issues with this type of test is that it is very reliant on the software calibration, and the end use of this system will have both the radar and target object in static positions. The new approach was to take two measurements with each antenna system: one measurement with a target object and another without. This way gave a comparison of how the system reacts to a

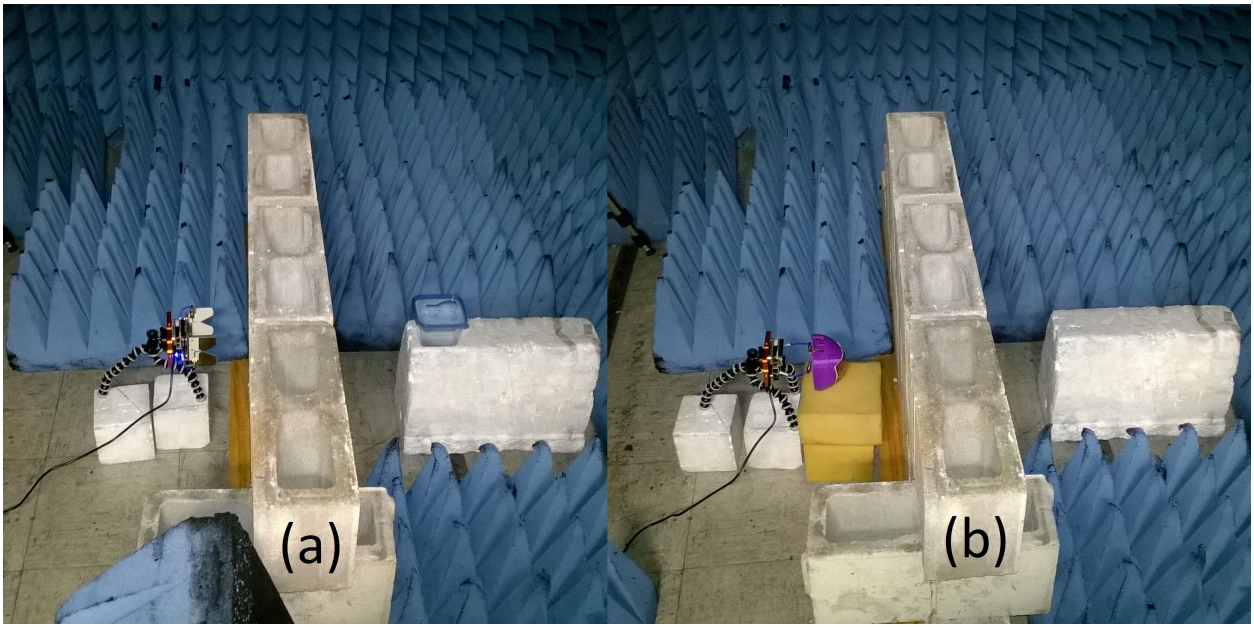

Figure 5.1. (a) Bow-tie with target object (b) Spiral conformal without target

target as well as how the systems compare to each other. To eliminate as much interference as possible, an RF anechoic chamber was used. A 42 cm high by 1 m long by 14 cm thick concrete wall was constructed using cinder blocks. The Cayenne radar along with the antenna under test was positioned approximately 6 cm away from the center of the wall as pictured in Figure 5.1.

The target object would be placed 30 cm directly across the wall from the radar shown in Figure 5.1 (a) where the bow-tie antenna is shown. The target object was a 10 cm x 10 cm x 7 cm plastic tub of water. The target would then be removed without modifying any other parameters in the room. Figure 5.1 (b) shows the conformal antennas with the target removed. The only variables between the tests were which antenna system was used and if the target object was in place or not.

5.4. Through Wall Testing Results

The raw B-Scan output was used to visually compare the two systems. These measurements were taken using a MATLAB code provided with the Salsa software and included an automatic calibration for the antenna. The resulting scans are shown in Figure 5.2.

There is a difference in signal strength between the spiral and bow-tie antennas. The darker horizontal lines shown in Figure 5.2 (a) and (b) indicate the bow-tie system received less background radiation when compared to the spiral system shown in Figure 5.2 (c) and (d). The B-Scan plots

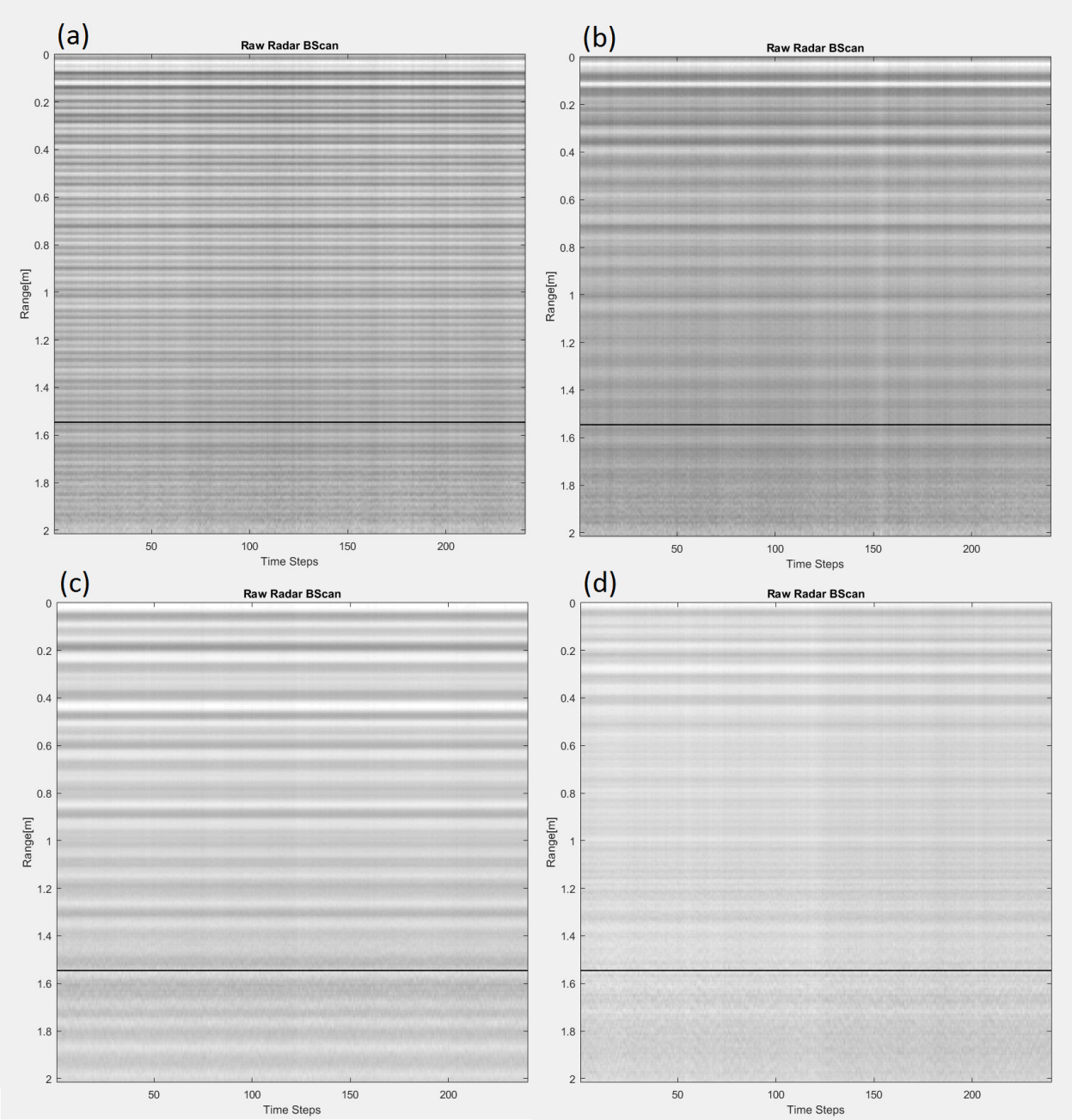

Figure 5.2. (a) Bow-tie without target (b) Bow-tie with target (c) Spiral without target (d) Spiral with target

the voltage values from the analog to digital converter from the received antenna of the radar. An increase in the power received will show an increase in voltage. As the voltage increases, the graphed lines will become more white. For example, if the radar was place in the anechoic chamber with no cinder block wall or target, the chamber walls will absorb most of the radar's transmitted power. The ideal B-Scan of this example would be completely black since the radar is not receiving

any power and the voltage would be zero. Inversely, if the radar would be placed in a metal box, most of the transmitted power would be received and the plots would be completely white. When comparing the bow-tie to the spiral without the target, Figure 5.2 (a) and (c) respectively, the bow-tie plot is darker. This indicates more of the spiral antenna's transmitted power was reflected off the cinder block wall and received by the radar. Thus, the bow-tie had better penetration through the wall.

When comparing the difference between the bow-tie without and with the target in place, Figure 5.2 (a) and (b) respectively, the plot appears to be more white. This indicates some of the transmitted power reflected off the target and was received by the radar. The spirals seem to have more of a reaction to placing the target in position as shown in Figure 5.2 (c) and (d). The plot in Figure 5.2 (d) shows more power reflected off the target and received by the radar. The larger difference in received power of the spiral system is preferred since a target can be more easily detected.

During the spiral antenna tests, if the target was moved to the left or right as little as 10 cm, the scan looked more as though the target was not there at all, but there was still a noticeable difference in the B-Scan output. This indicates the spiral antennas are more directional. The use of directional antennas with the radar can be beneficial in locating the exact position of the target. However, the more directional the antenna is, the less area it will be able to scan, thus requiring more radar systems. The objective was to show the spiral system can behave as well as the bow-tie and these initial readings seems to indicate that it does.

6. CONCLUSIONS

The design, simulation, and analysis of a conformal spiral antenna design was shown in this work. This design was then successfully integrated with the Flat Earth Inc. Cayenne radar development kit [8]. A planar spiral shape was initially designed and simulated in HFSS and then super-imposed onto a 127 mm hemispherical surface. It was shown the conformal antenna had a simulated -10 dB bandwidth of over 8.0 GHz and a gain of 7.58 dB. A microstrip tapered balun impedance transformer was also designed and simulated to feed the antennas from the unbalanced 50 Ω input. The -10 dB bandwidth of the conformal antennas was measured to be 3.0 GHz with a peak gain of 1.9 dBi. It was show the spirals had less return loss, but less gain in the lower frequencies when compared to the bow-tie antennas. When the two systems were compared using the Cayenne radar, the initial tests indicate there is little difference between the two. This work presents a platform for which future UWB radar conformal antenna designs can based.

REFERENCES

[1] Novelda Xethru, https://www.xethru.com/, accessed March 2016

[2] E.M. Staderini: 'UWB radars in medicine', *IEEE Aerospace and Electronic Systems Mag., vol. 17, no. 1*, 2002, pp. 13 - 18

[3] I. Immoreev: 'UWB Radar for Patient Monitoring', *IEEE Aerospace and Electronic Systems Mag., vol. 23, no. 11*, 2006, pp. 11 - 18

[4] Camero Tech Ltd., http://www.camero-tech.com/, accessed March 2016

[5] A.G. Yarovoy, L.P. Lighart, J. Matuzas, B. Levitas: 'UWB Radar for Human Being Detection', *IEEE Aerospace and Electronic Systems Mag., vol. 21, no. 3*, 2006, pp. 10 - 14

[6] Cyclops Technologies, http://cyclopstechnologies.co/, accessed March 2016

[7] D. T. Wisland, S. Stoa, N. Andersen, K. Granhaug, T.S. Lande, H.A. Hjortland: 'CMOS nanoscale impulse radar utilized in 2-dimensional ISAR imaging system', *IEEE Radar Conference (RADAR)*, 2012, pp. 714 - 719

[8] Flat Earth Inc., http://www.flatearthinc.com/, accessed March 2016

[9] C. A. Balanis: 'Antenna Theory Analysis and Design third edition', (John Wiley and Sons Inc, Hoboken NJ, 2005), pp. 615 - 616

[10] W. L. Stutzman, G. A. Thiele: 'Antenna Theory and Design third edition', (John Wiley and Sons Inc, Hoboken NJ, 2013), pp. 245 - 251

[11] Rogers Corporation, http://http://www.rogerscorp.com/, accessed March 2016

[12] High Frequency Structural Simulator (HFSS), http://www.ansys.com/, accessed March 2016

[13] K. Vinyaygamoorthy, J. Coetzee, D. Jayalath: 'Microstrip to Parallel Strip Balun as Spiral Antenna Feed', *Vehicular Technology Conference, 2012 IEEE 75th*, 2012, pp. 1 - 5

[14] Computer Simulation Technology Microwave Studios (CST), http://www.cst.com/, accessed March 2016

[15] G. Wenjun, L. Miao, L. Shanwei: 'Numerical Calculation of a Tchebycheff Tapered Balun Transformer', *International Conference on Computational Electromagnetics and its Applications*, 1999, pp. 402 - 405

APPENDIX. MATLAB GAIN PLOT

```
% ***This script will require the RF Toolbox***
% This script plots the gain of an antenna using provided SNP measurements
% Note: This file requires three inputs as described below:
% 1) S2P file of the S21 reference antenna measurement
% 2) S2P file of the S21 antenna under test measurement
% 3) CSV file of the reference antenna gain (from datasheet)
% Note: Both the S21 measurements should be the same frequency range since
% the measurements should be taken using the exact same VNA state file.
% The CSV file can be any frequency range or number of points.
% Input the reference antenna .s2p file and rename
REF = sparameters('file\path\here\Ref_Ant.SNP');
% Input the antenna under test .s2p file and rename
AUT = sparameters('file\path\here\AUT_Ant.SNP');
% Input the CSV file of the reference antenna's gain
M = csvread('F:\DefaultDataset.csv');
% Extract the frequency vectors from both
FreqREF = REF.Frequencies;
FreqAUT = AUT.Frequencies;
% Extract the frequency from CSV
X = M(:,1).*1e9;
% Extract S21 from both and convert to dB
S21_REF = 20*log10(abs(rfparam(REF,2,1)));
S21_AUT = 20*log10(abs(rfparam(AUT,2,1)));
% Extract the gain (dBi) from the CSV
Y = M(:,2);
% Find number of points of SNP
pts = length(FreqREF);
% Find min frequency of SNP
Fmin = min(FreqREF);
% Find max frequency of SNP
Fmax = max(FreqREF);
% Create new frequency span for CSV
Xp = linspace(Fmin,Fmax,pts);
% Initiate counter variable
i = 1;
% This loop makes adds more points to the input of the CSV file to make the
% vector the same length as the SNP vectors
while i <= pts
    % Finds the correct matrix index to match the frequency between CSV and
    % SNP files
    K(i,:) = abs(Xp(i) - X);
    % Rounds the matched index to the nearest frequency point from the CSV
    [Km(i) Kp(i)] = min(K(i,:));
    % Use the index value to create new frequency array
    Yp(i) = Y(Kp(i));
    % Increase counter
    i = i+1;
end
% Gain equation. Yp must be transposed to add correctly
Gain1 = S21_AUT -S21_REF + Yp';
% Plot gain over frequency
plot(FreqREF,Gain1)
xlabel('Frequency (GHz)');
ylabel('Gain (dBi)');
```